Electronic supporting Information

Stabilized Inverse Y_2O_3/Cu Interfaces Boosted the Performance of Reverse Water-Gas Shift Reaction

Zhi-Xin Li, Kai Xu, Wei-Wei Wang, Xin-Pu Fu, Chun-Jiang Jia*

Key Laboratory for Colloid and Interface Chemistry, Key Laboratory of Special Aggregated Materials, School of Chemistry and Chemical Engineering, Shandong University, Jinan, 250100, China.

*Corresponding Author. Email: jiacj@sdu.edu.cn

Experimental Section

Materials. $Cu(NO_3)_2 \cdot 3H_2O$, $Y(NO_3)_3 \cdot 6H_2O$, Y_2O_3, $Cu(OH)_2$, ethanol and anhydrous sodium carbonate were from Sinopharma Chemical Reagent Co., Ltd (the purity of all drugs were 99.9%). All gases used in the study were purchased from Jinan Deyang Special Gases Co., Ltd.

Catalyst preparation. Preparation of bare Cu catalyst. Usually, a certain amount of $Cu(NO_3)_2 \cdot 3H_2O$ solution (0.01 $g \cdot mL^{-1}$) and sodium carbonate solution (0.5 $mol \cdot L^{-1}$) were added to 25 mL deionized water at the same time drop by drop at room temperature, and the pH value of the mixture was always 10.0. Then the blue mixture was stirred for 30 min and aged for 1 h. Next, the blue precipitates (The precursor of bare Cu catalyst) were obtained after filtering, washing and drying. The blue precipitates were calcined in Muffle furnace at 400 °C for 4 h to obtain the bare Cu catalyst. Additional commercial $Cu(OH)_2$ or $Cu(NO_3)_2 \cdot 3H_2O$ was calcined in Muffle furnace at 400 °C for 4 h to obtain the bare Cu_{-C} or Cu_{-N} catalysts, respectively. The Y_2O_3/Cu-CP and Cu/Y_2O_3-CP catalyst was prepared by co-precipitation method. A certain amount of $Cu(NO_3)_2 \cdot 3H_2O$ solution (0.01 $g \cdot mL^{-1}$) and $Y(NO_3)_3 \cdot 6H_2O$ solution (0.01 $g \cdot mL^{-1}$) were simultaneously added to 25 ml deionized water, and the pH was adjusted to 10.0 by sodium carbonate solution (0.5 $mol \cdot L^{-1}$). After the same process as that of bare Cu catalyst, Y_2O_3/Cu-CP and Cu/Y_2O_3-CP catalyst was obtained.

Supplementary Figures:

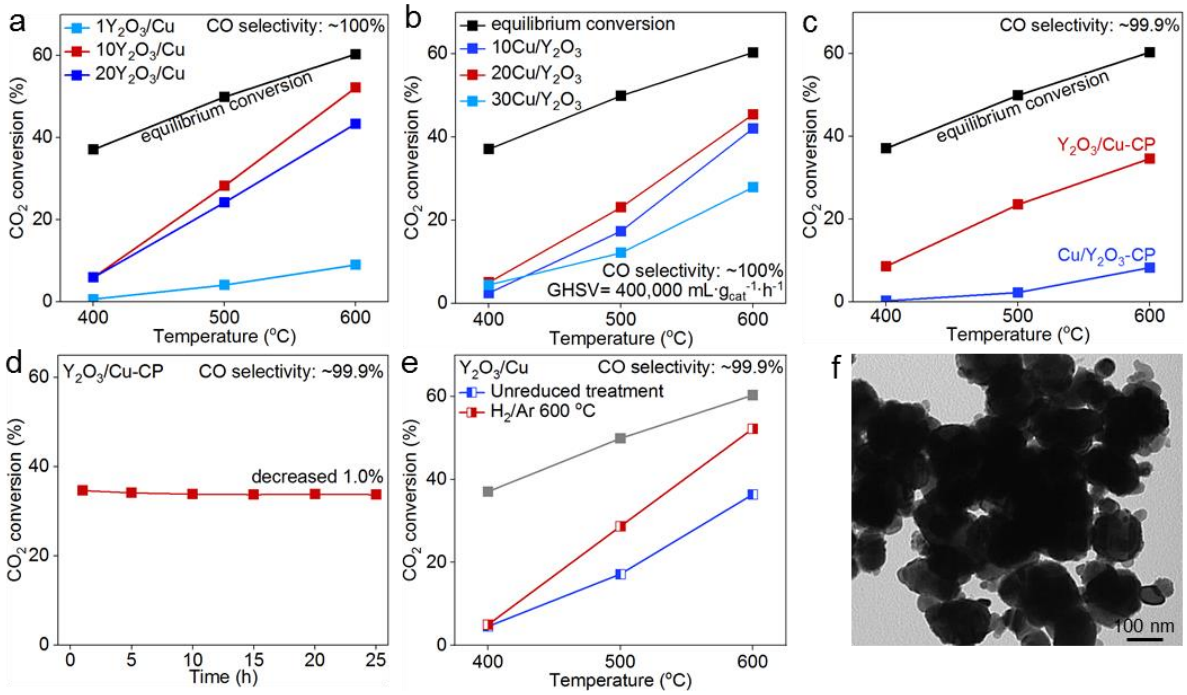

Fig. S1. RWGS reaction performance over (a) inverse Y_2O_3/Cu and (b) conventional Cu/Y_2O_3 catalysts (calcination at 400 °C). (c) RWGS reaction performance over inverse Y_2O_3/Cu-CP and conventional Cu/Y_2O_3-CP catalysts constructed by co-precipitation. (d) Long-term stability of inverse Y_2O_3/Cu-CP catalysts constructed by co-precipitation in RWGS reaction. (e) RWGS reaction performance over as-prepared Y_2O_3/Cu catalyst without reduction treatment. (f) TEM images of as-prepared Y_2O_3/Cu catalyst (without reduction treatment) after reaction. (Reaction condition: 23%CO_2/69%H_2/8%N_2, GHSV = 400,000 mL·g_{cat}^{-1}·h^{-1})

CO_2 conversion of the inverse Y_2O_3/Cu catalysts increased first and then decreased with increasing of Y element loading, which might be caused by overloading of the active site (**Fig. S1a**). There was no significant improvement in catalytic performance while the Cu load of conventional Cu/Y_2O_3 catalysts increased from 10 to 20% (**Fig. S1b**). Conventional Cu/Y_2O_3-CP (The mass ratio of Cu to Y_2O_3 was 1: 9) and inverse Y_2O_3/Cu-CP (The mass ratio of Cu to Y_2O_3 was 9: 1) catalysts were prepared by co-precipitation method (**Fig. S1c** and **d**). As shown in **Fig. S1c** and **d**, the CO_2 conversion of inverse Y_2O_3/Cu-CP catalyst (34.6%) constructed by co-precipitation was still higher than conventional Cu/Y_2O_3-CP catalyst (8.3%) constructed by co-precipitation at 600 °C, and inverse Y_2O_3/Cu-CP catalyst exhibited excellent long-term stability, which also confirmed that the inverse Y_2O_3/CuO_x/Cu interfaces played an important role in RWGS reaction. As shown in **Fig. S1e**, when as-prepared sample with highly dispersed Y species were directly used for catalyzing the RWGS reaction without reduction treatment, its CO_2 conversion was poor, especially only 36.4% at 600 °C, which was much lower than the catalytic activity after 5%H_2/Ar pretreatment (52.3% at 600 °C). In addition, it transformed into the inverse structure with small particles (Y_2O_3) embedded on surface of large particles (Cu) after reaction (**Fig. S1f**). It was noteworthy that the small particles size exceeded 20 nm, indicated that highly dispersed Y species has been occurred severe agglomeration, which might cause by violent reduction of the high concentration of H_2 (69%H_2) in reaction atmosphere. Therefore, the severe agglomeration might lead to a serious loss of interface sites, thereby reducing catalytic activity.

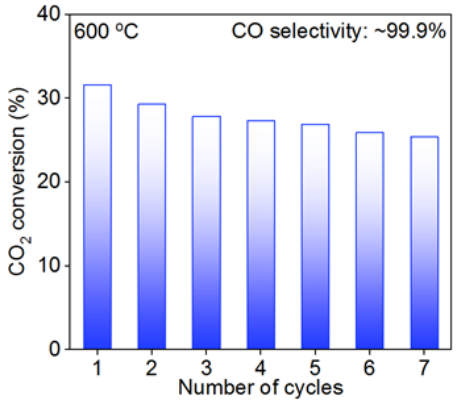

Fig. S2. Recycling performance of conventional Cu/Y_2O_3 catalyst. (Reaction condition: $23\%CO_2/69\%H_2/8\%N_2$, GHSV = 400,000 $mL \cdot g_{cat}^{-1} \cdot h^{-1}$)

The cold start recycling performance of conventional Cu/Y_2O_3 catalyst was poor, and the CO_2 conversion decreased by 6.2% after 7 cycles at 600 °C.

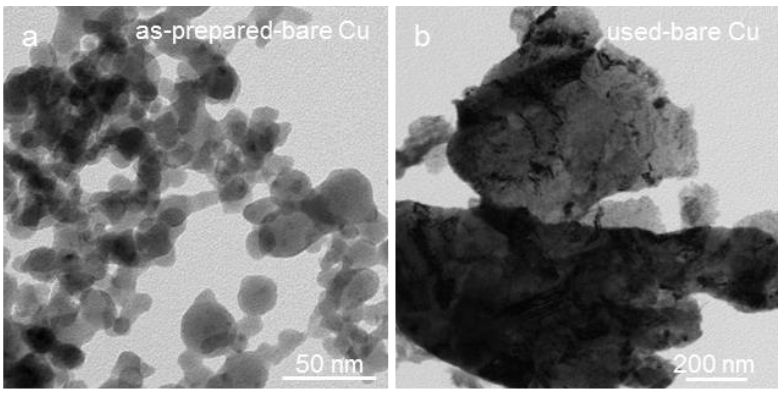

Fig. S3. TEM images of bare Cu catalyst.

As shown in **Fig. S3a**, as-prepared bare Cu catalyst was the about 20−40 nm of particles. After reaction, the Cu NPs agglomerated and grown significantly (**Fig. S3b)**.

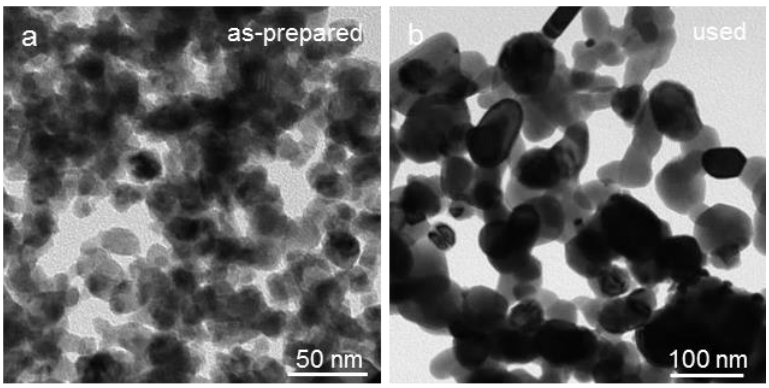

Fig. S4. TEM images of conventional Cu/Y_2O_3 catalyst.

As shown in **Fig. S4a**, as-prepared conventional Cu/Y_2O_3 catalyst was the particle about 20−40 nm. After reaction, the conventional Cu/Y_2O_3 catalyst agglomerated and grown significantly (**Fig. S4b)**.

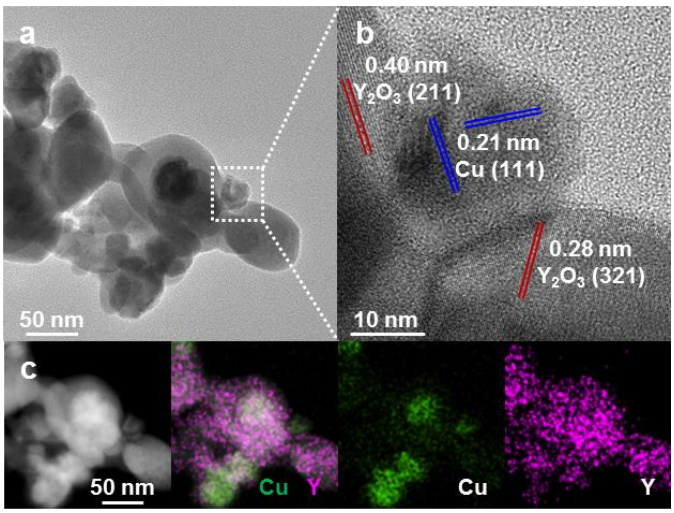

Fig. S5. TEM, HRTEM and EDS element mapping images of used conventional Cu/Y_2O_3 catalyst.

In **Fig. S5a**, the used conventional Cu/Y_2O_3 catalyst was the particle about 10−100 nm. HRTEM image displayed that the surface of the small particles in **Fig. S5a** had the lattice fringes with clear spacing of 0.21 nm, which could be attributed to Cu (111) (**Fig. S5b)**. Additional the HRTEM image displayed that the surface of the large particle in **Fig. S5a** had the lattice fringes with clear spacing of 0.28 and 0.40 nm, which could be attributed to Y_2O_3 (321) and Y_2O_3 (211), respectively (**Fig. S5b)**. EDS element mapping images also clearly shown that Cu NPs was embedded on the surface of Y_2O_3 NPs (**Fig. S5c)**. These results indicated that Cu NPs embedded on Y_2O_3 NPs constituted a clear interface structure.

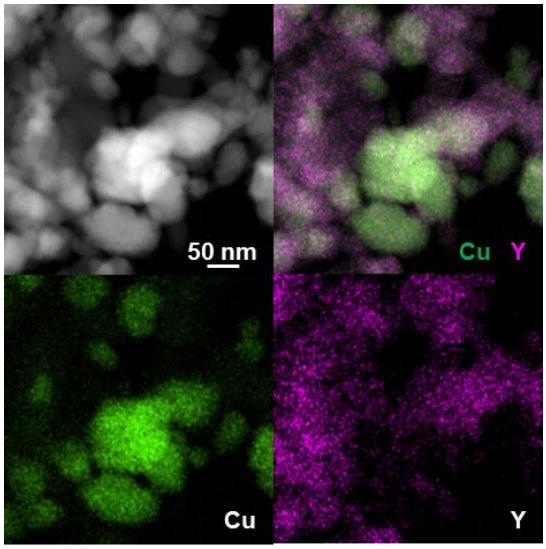

Fig. S6. EDS element mapping images of the used conventional Cu/Y_2O_3 catalyst.

EDS element mapping images shown that the Cu NPs (10−50 nm) were seriously agglomerated on the surface of Y_2O_3, implying the conventional Cu/Y_2O_3 interface on conventional Cu/Y_2O_3 catalyst might be unevenly dispersed.

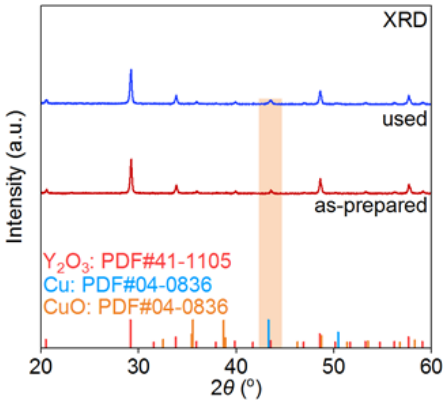

Fig. S7. XRD patterns of conventional Cu/Y_2O_3 catalyst.

XRD patterns displayed that as-prepared and used conventional Cu/Y_2O_3 catalysts exhibited a significant Y_2O_3 (PDF#41-1105) characteristic diffraction peak. There was no diffraction peak of Cu species, which might be caused by low loading or better dispersion.

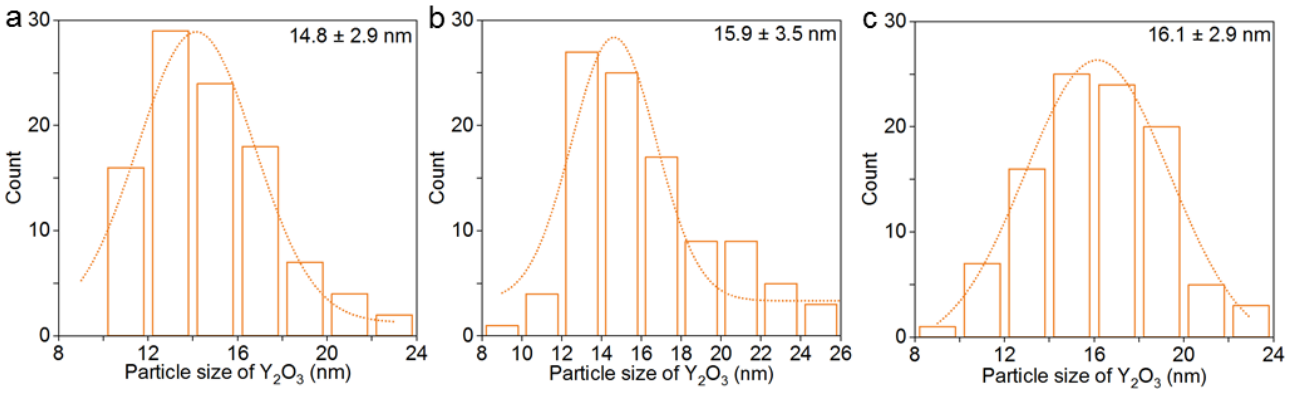

Fig. S8. Statistical diagram of Y_2O_3 NPs size on inverse Y_2O_3/Cu catalyst operated for (a) 1 h, (b) 20 h and (c) 100 h at 600 °C, where the corresponding TEM images were shown in **Fig. 4a–c**.

The size of Y_2O_3 NPs on the surface of inverse Y_2O_3/Cu catalyst was 14.8 nm after reaction (**Fig. 8a**). The size of Y_2O_3 NPs increased to 15.9 nm and 16.1 nm after long-term stability tests for 20 h (**Fig. 8b**) and 100 h (**Fig. 8c**).

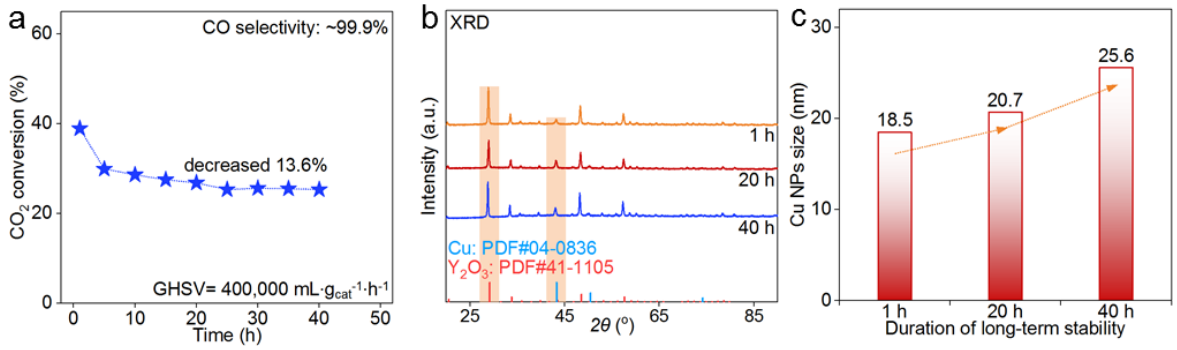

Fig. S9. (a) The long-term stability at 600 °C, (b) XRD patterns and (c) the average size of Cu NPs for conventional 20Cu/Y_2O_3 catalyst.

Since the diffraction peak of Cu species was not detected in XRD patterns of the conventional Cu/Y_2O_3 catalyst with a loading capacity of 10%, the conventional Cu/Y_2O_3 catalyst with a loading capacity of 20% was explored here. After a long-term stability test of up to 40 h, the CO_2 conversion of conventional 20Cu/Y_2O_3 catalysts was decreased by more than 13.6% (**Fig. S9a)**. XRD patterns displayed that the used conventional 20Cu/Y_2O_3 catalysts exhibited a significant Y_2O_3 (PDF#41-1105) characteristic diffraction peak (**Fig. S9b)**. The intensity of characteristic diffraction peak at 43.3° did not match the Y_2O_3 on XRD patterns of conventional 20Cu/Y_2O_3 catalyst (**Fig. S9b)**, which might be the characteristic diffraction peak of metal Cu (PDF#04-0836). The remarkable agglomeration of Cu NPs could be observed on the conventional 20Cu/Y_2O_3 catalyst by calculating the Cu NPs size under different treatment conditions (Scherrer formula). The size of Cu NPs on conventional 20Cu/Y_2O_3 catalyst after reaction was 18.5 nm, which increased significantly to 20.7 nm after reaction for 20 h (**Fig. S9c**). When the reaction time was 40 h, the size of Cu NPs was stable at 25.6 nm.

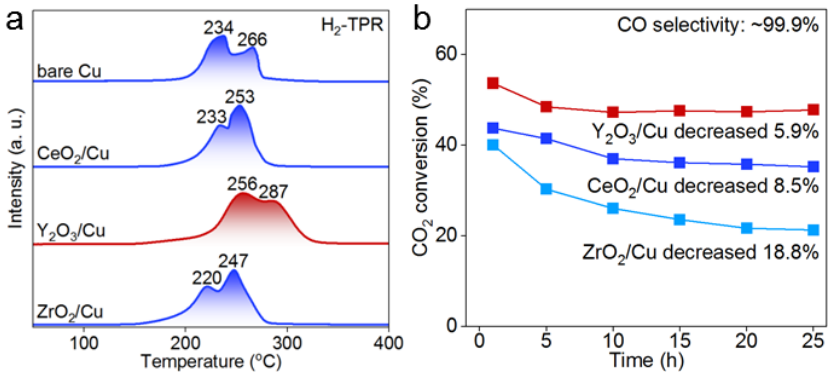

Fig. S10. (a) H_2-TPR profiles of various catalysts. (b) Long-term stability of RWGS reaction over various catalysts. (Reaction condition: 23%CO_2/69%H_2/8%N_2, GHSV = 400,000 mL·g_{cat}^{-1}·h^{-1})

The metal-support interaction of the prepared comparable CeO_2/Cu and ZrO_2/Cu catalysts was weaker than that of Y_2O_3/Cu catalyst (**Fig. S10a**), so the long-term stability of CeO_2/Cu and ZrO_2/Cu catalysts is relatively poor (**Fig. S10b**).

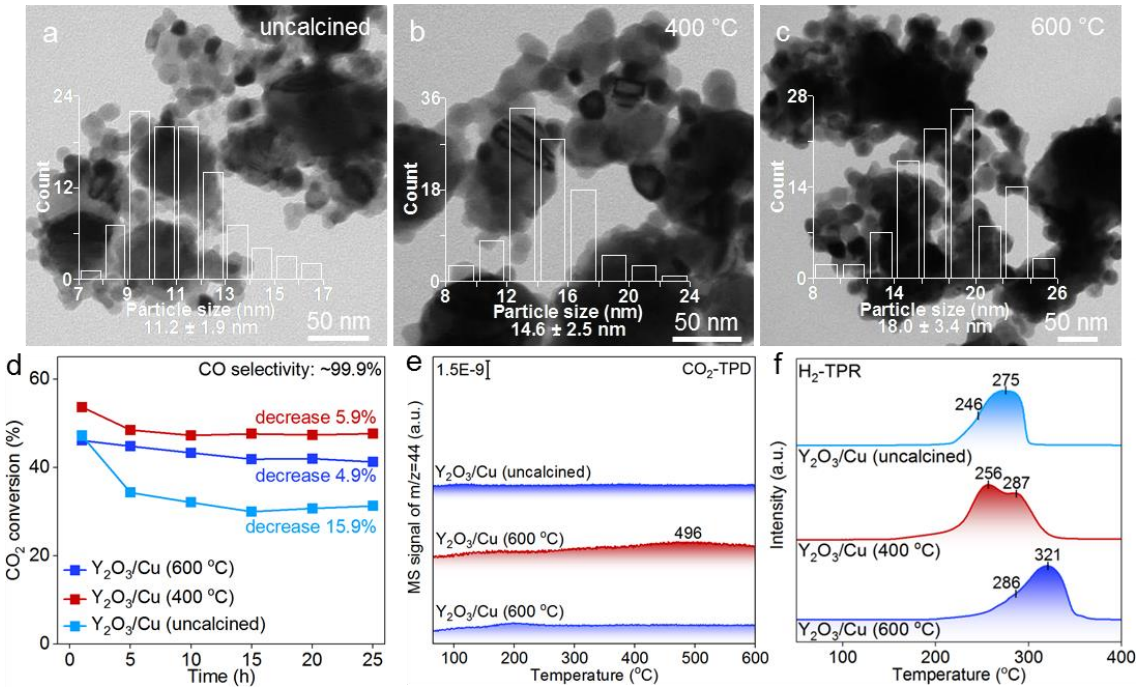

Fig. S11. (a–c) TEM images of used inverse Y_2O_3/Cu catalysts prepared at different calcination temperatures. (d) Long-term stability of RWGS reaction over various catalysts. (Reaction condition: 23%CO_2/69%H_2/8%N_2, GHSV = 400,000 mL·g_{cat}^{-1}·h^{-1}). (e) CO_2-TPD profiles of various catalysts. (f) H_2-TPR profiles of various catalysts.

The Y_2O_3/Cu (uncalcined), Y_2O_3/Cu (400 °C, the inverse Y_2O_3/Cu catalyst in manuscript) and Y_2O_3/Cu (600 °C) catalysts were prepared by adjusting the calcination temperature, where the Y_2O_3 size of Y_2O_3/Cu (uncalcined), Y_2O_3/Cu (400 °C) and Y_2O_3/Cu (600 °C) catalysts after reaction were 11.2, 14.6 and 18.0 nm (**Fig. S11a–c**). The CO_2 conversion of catalyst Y_2O_3/Cu (uncalcined) and Y_2O_3/Cu (600 °C) was significantly lower than Y_2O_3/Cu (400 °C) catalyst (**Fig. S11d**). Meanwhile, **Fig. S11e** indicated that CO_2 adsorption capacity of Y_2O_3/Cu (400 °C) catalyst was excellent than Y_2O_3/Cu (uncalcined) and Y_2O_3/Cu (600 °C) catalysts, which was consistent with the catalytic activity (**Fig. S11d**). These results indicated that only appropriate Y_2O_3 size could promote the adsorption of CO_2 to improve the catalytic activity. In addition, **Fig. S11d** indicated that the long-term stability of Y_2O_3/Cu catalysts gradually increased with raising the calcination temperature. After reaction for 25 h, Y_2O_3/Cu (600 °C) catalyst showed the best long-term stability with decreasing of only 4.9%. Meanwhile, H_2-TPR profiles (**Fig. S11f**) shown that with raising calcination temperature, the reduction temperature of Y_2O_3/Cu catalysts also increased gradually, indicating that the metal-support interaction was enhanced, which was consistent with the results of catalytic stability (**Fig. S11d**). Therefore, it was again confirmed that Cu-Y_2O_3 interaction generated by interface could improve catalytic stability. However, the strength of metal-support interaction (**Fig. S11f**) did not match the CO_2 adsorption capacity (**Fig. S11e**), illustrating that there was no convincing law between metal-support interaction and CO_2 adsorption strength. In other words, only the appropriate metal-support interaction could promote the adsorption of CO_2 to improve the catalytic activity.

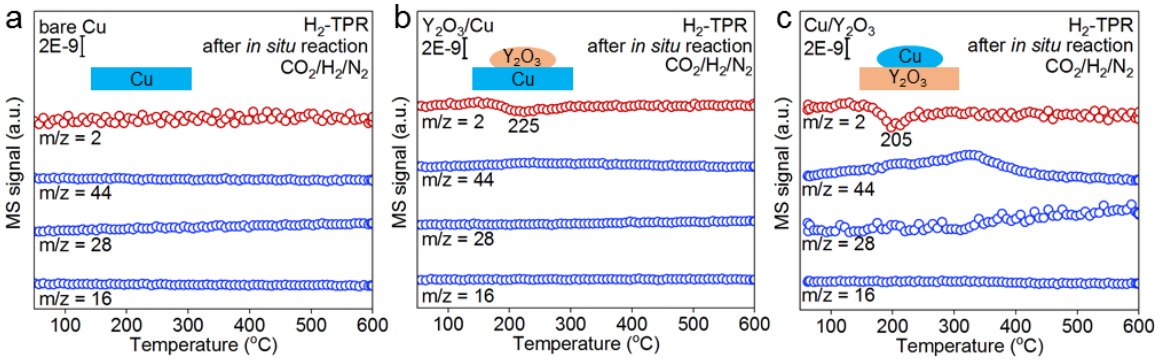

Fig. S12. H_2-TPR profiles collected after *in situ* reaction at 600 °C for 1 h in a mixed-gas (23%CO_2/69%H_2/8%N_2) over bare Cu, inverse Y_2O_3/Cu and conventional Cu/Y_2O_3 catalysts.

There was no H_2 consumption signal in the H_2-TPR profiles of bare Cu catalyst after reaction at 600 °C in mixed-gas (23%CO_2/69%H_2/8%N_2) for 1 h (**Fig. S12a**). The H_2-TPR profiles of inverse Y_2O_3/Cu and conventional Cu/Y_2O_3 catalyst after reaction at 600 °C in mixed-gas (23%CO_2/69%H_2/8%N_2) for 1 h showed a clear H_2 consumption signal (m/z = 2) at 150−300 °C without any hydrogenation product formation, suggesting the $Cu^{\delta+}$ species might be reduced (**Fig. S12b** and **12c**).

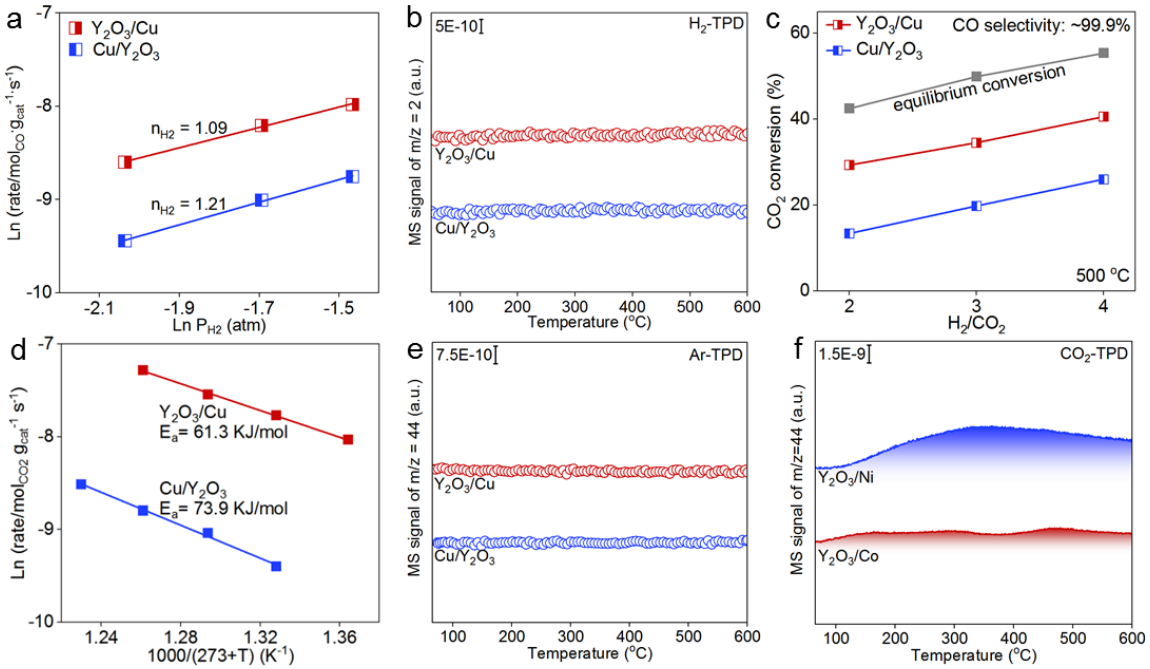

Fig. S13. (a) The H_2 reaction order (600 °C, the detailed data were summarized in **Table S4**), (b) H_2-TPD profiles of Y_2O_3/Cu and Cu/Y_2O_3 catalysts. (c) RWGS reaction performance in mixed gas with different CO_2/H_2 ratios (Reaction condition: The content of CO_2 in mixed gas is 10%, GHSV = 400,000 mL·g_{cat}^{-1}·h^{-1}), (d) Arrhenius plots in kinetic range (The detailed data were summarized in **Table S5**) and (e) Ar-TPD and (f) CO_2-TPD profiles of various catalysts.

The H_2 reaction order of inverse Y_2O_3/Cu catalyst was significantly lower than conventional Cu/Y_2O_3 catalyst (**Fig. S13a**), which indicated that the inverse Y_2O_3/Cu catalyst was conducive to improving the adsorption and activation capacity of H_2. The H_2-TPD profiles (**Fig. S13b**) confirmed that the H_2 adsorption capacity of inverse Y_2O_3/Cu and conventional Cu/Y_2O_3 catalysts was very weak. In addition, with increasing of H_2 content in mixed gas, the CO_2 conversion of both inverse Y_2O_3/Cu and conventional Cu/Y_2O_3 catalysts continued to increase (**Fig. S13c**), indicating that the concentration of H_2 played the important role in improving the RWGS reaction performance. The lower activation energy of the inverse Y_2O_3/Cu catalyst also indicated that it was more conducive to promoting the occurrence of RWGS reaction (**Fig. S13d**). Inverse Y_2O_3/Cu and conventional Cu/Y_2O_3 catalysts did not decompose to produce the signal of CO_2 (**Fig. S13e**). The inverse Y_2O_3/Co and Y_2O_3/Ni catalysts constructed by Ni and Co metals and Y_2O_3 also had excellent CO_2 adsorption capacity (**Fig. S13f**), indicated that Y_2O_3 could effectively improve the CO_2 adsorption capacity of inverse catalysts.

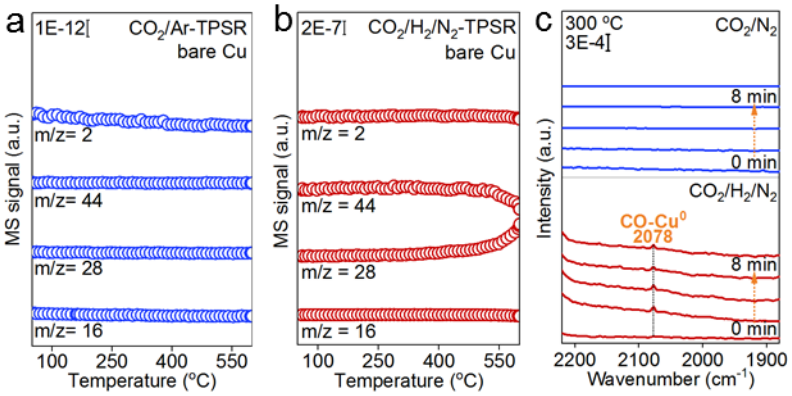

Fig. S14. TPSR results of bare Cu catalyst in (a) 2%CO_2/98%N_2 and (b) 23%CO_2/69%H_2/8%N_2. (c) *In situ* DRIFTS spectra of Cu/Y_2O_3 catalyst collected in 2%CO_2/98%N_2 and 23%CO_2/69%H_2/8%N_2 at 300 °C.

There was no CO generation signal in CO_2/Ar, while significant CO generation signal appeared in CO_2/H_2/N_2 before 500 °C, indicating that the synergistic reaction mechanism was followed on bare Cu catalyst (**Fig. S14a and b**). There was no CO related signal on *In situ* DRIFTS spectra of Cu/Y_2O_3 catalyst collected in CO_2/Ar, while significant CO-Cu^0 signal (2078 cm^{-1}) appeared on *In situ* DRIFTS spectra of Cu/Y_2O_3 catalyst collected in CO_2/H_2/N_2 (The absence of CO gas signal might be caused by the poor activity of Cu/Y_2O_3 catalyst), indicating that the synergistic reaction mechanism was followed on Cu/Y_2O_3 catalyst (**Fig. S14c**).

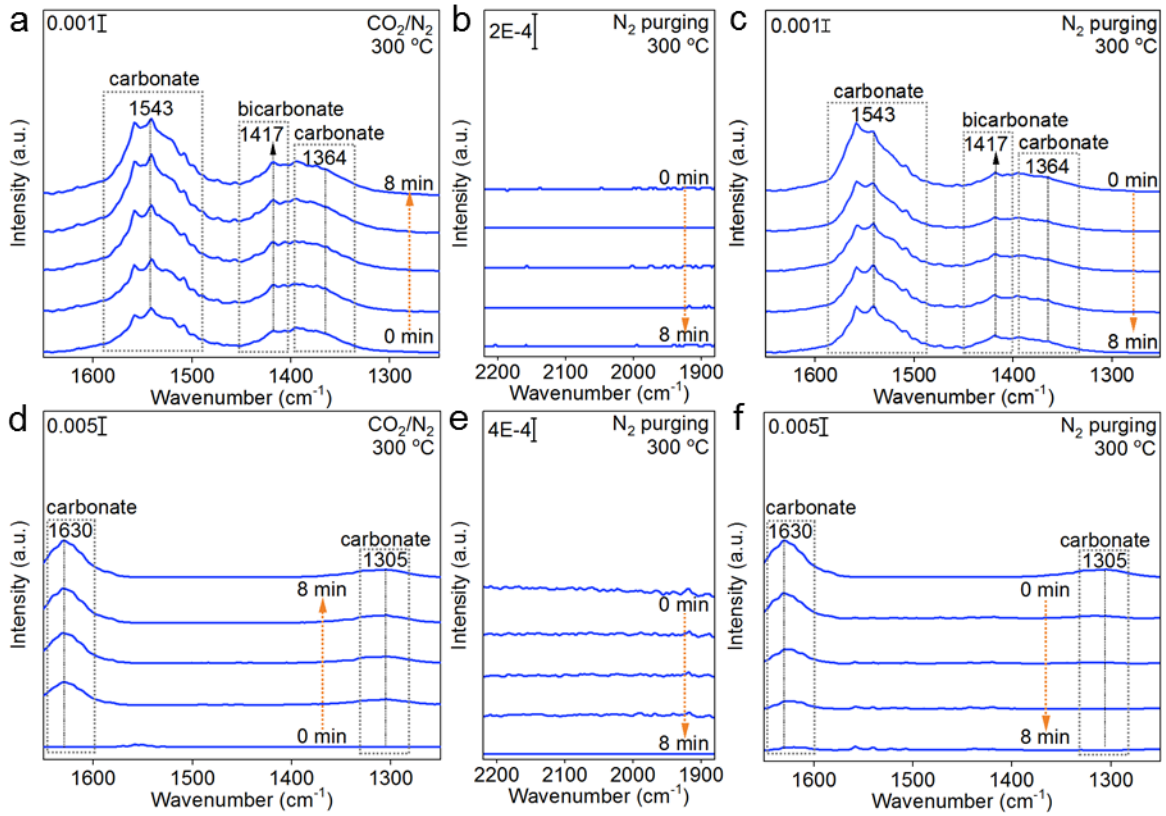

Fig. S15. *In situ* DRIFTS spectra of inverse Y_2O_3/Cu catalyst collected in (a) 2%CO_2/98%N_2 and (b,c) N_2 after 2%CO_2/98%N_2 pretreatment at 300 °C. *In situ* DRIFTS spectra of conventional Cu/Y_2O_3 catalyst collected in (a) 2%CO_2/98%N_2 and (b,c) N_2 after 2%CO_2/98%N_2 pretreatment at 300 °C.

In situ DRIFTS spectra showed that there were significant carbonate species on both the inverse Y_2O_3/Cu catalyst (**Fig. S15a**, 1364, 1417 and 1543 cm^{-1}) and conventional Cu/Y_2O_3 catalyst (**Fig. S15d**, 1305 and 1630 cm^{-1}), indicating that both catalysts could achieve effective CO_2 activation. However, when switching to high purity N_2 gas purge, the inverse Y_2O_3/Cu catalyst (**Fig. S15b and S15c**) showed a relatively stronger CO_2 adsorption capacity than conventional Cu/Y_2O_3 catalyst (**Fig. S15e and S15f**), which was consistent with the results of CO_2-TPD (**Fig. S6**).

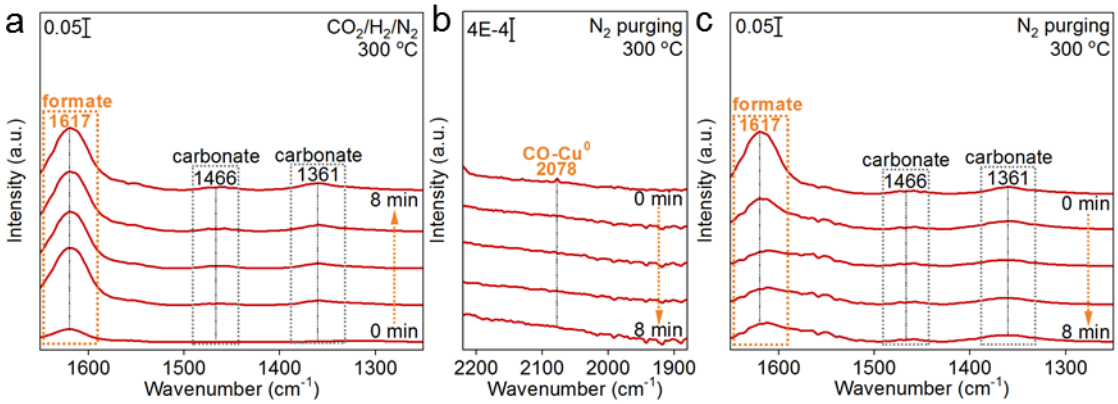

Fig. S16. *In situ* DRIFTS spectra of conventional Cu/Y_2O_3 catalyst collected in (a) 23%CO_2/69%H_2/8%N_2 and (b,c) N_2 after 23%CO_2/69%H_2/8%N_2 pretreatment at 300 °C.

In situ DRIFTS spectra further clarified the RWGS reaction mechanism on conventional Cu/Y_2O_3 catalyst. As shown in **Fig. S16a**, the carbonate (1361 and 1466 cm^{-1}) and formate (1617 cm^{-1}) signal appeared on the *in situ* DRIFTS spectra in 23%CO_2/69%H_2/8%N_2 at 300 °C. When switching to N_2 purge, the CO-Cu^0 signals (**Fig. S16b,** 2078 cm^{-1}) rapidly decreased, while the signal strength of carbonate (1361 and 1466 cm^{-1}) and formate (1617 cm^{-1}) (**Fig. S16c**) also slowly decreased. These findings further revealed that the RWGS reaction followed a synergistic reaction path on conventional Cu/Y_2O_3 catalyst.

Supplementary Tables:

Table S1. Comparison of reaction rates of various catalysts.

Entry	Samples	Temperature	Reaction rate ($mmol_{CO}/g_{cat}/s$)	References
1	Inverse Y_2O_3/Cu	500	529.9	This work
2	Conventional Cu/Y_2O_3	500	144.7	This work
3	bare Cu	500	3.1	This work
4	Cu-Zn-Al	500	261.0	[1]
5	Cu-Al spinel	600	179.0	[2]
6	Pt/TiO_2	400	50.0	[3]
7	Cu-CeO_2	500	46.6	[4]
8	TiO_2/Cu	500	17.8	[5]
9	NP-Cr_2O_3/Cu	400	19.7	[6]

Table S2. Related parameters of various catalysts.

Samples	S_{BET} (m^2/g) [a]	Atomic (%) [b]			Size of NPs (nm) [c]	
		Y	Cu	O	Cu NPs	Y_2O_3 NPs
Conventional Cu/Y_2O_3-used	40.0	29.7	9.6	60.7	-	34.5
Inverse Y_2O_3/Cu-used	41.5	21.6	33.5	44.9	31.5	14.8

[a] Calculated by the BET method. [b] Characterized by XPS. [c] The value was obtained by Scherrer formula and XRD patterns.

The Cu NPs size of used inverse Y_2O_3/Cu calculated by XRD (31.5 nm) was much smaller than that observed by TEM (> 100 nm). The super-sized Cu NPs observed in TEM image might be caused by the agglomeration of several small Cu NPs.

Table S3. Estimation of the number of interfaces on the surface of catalysts.

Samples	Interface sites			Deactivation ratio (%) [b]
	used	used (20 h)	used (100 h)	
Conventional Cu/Y_2O_3 [a]	3.1×10^{18}	2.2×10^{18}	1.4×10^{18}	53.0
Inverse Y_2O_3/Cu	5.2×10^{18}	3.9×10^{18}	3.2×10^{18}	39.3

[a] There were no significant characteristic diffraction peaks of Cu species on XRD pattern of conventional Cu/Y_2O_3 catalyst due to the low load, so only the number of interface sites on conventional $20Cu/Y_2O_3$ catalyst was calculated.

[b] The deactivation ratio referred to the ratio for number of decreased interface sites (100 h) to initial interface sites.

The detailed calculation process for number of interface sites was as follows: Under ideal conditions, the number of interfacial sites (A) for inverse Y_2O_3/Cu could be measured by the number of Cu atoms at the interface.[7-9] The perimeter of the Y_2O_3-Cu interface was ideally thought to be equal to the maximum perimeter of Y_2O_3 NPs (Y_2O_3 NPs were ideally thought to be spherical). Therefore, it was only necessary to calculate the number of Cu atoms in the maximum circumference of Y_2O_3 NPs, and the number of interfacial sites of each Y_2O_3 NPs of catalyst could be obtained. The number of interfacial sites on conventional Cu/Y_2O_3 catalyst was calculated by using the same method.[7-9] The number of interface sites on 1 g catalyst was calculated in Table S3.

Table S4. Raw data of reaction order results for various catalysts.

Reaction order	Catalyst	CO_2 conv. (%)	Flow (mL/min)	Ln P_{H2} (atm)	CO_2 content (%)	Rate (mol/s/gcat)	Ln(Rate)
H_2	Cu/Y_2O_3	7.46	46	-2.04	65.2	7.93E-05	-9.44
		11.52	49	-1.69	61.2	1.22E-04	-9.01
		14.85	52	-1.47	57.7	1.58E-04	-8.75
	Y_2O_3/Cu	8.25	46	-2.04	65.2	1.84E-04	-8.60
		12.25	49	-1.69	61.2	2.73E-04	-8.20
		15.32	52	-1.47	57.7	3.42E-04	-7.98
CO_2	Cu/Y_2O_3	14.30	35	-1.25	28.6	9.67E-05	-9.24
		12.23	40	-0.98	37.5	1.24E-04	-8.99
		10.45	45	-0.81	44.4	1.41E-04	-8.86
	Y_2O_3/Cu	13.45	35	-1.25	28.6	3.45E-04	-7.97
		10.45	40	-0.98	37.5	4.02E-04	-7.82
		8.88	45	-0.81	44.4	4.56E-04	-7.69

Notes: CO select. = 100%; H_2 reaction order: $m_{cat.}$ (Cu/Y_2O_3) = 21.0 mg, $m_{cat.}$ (Y_2O_3/Cu) = 10.0 mg; CO_2 reaction order: $m_{cat.}$ (Cu/Y_2O_3) = 11.0 mg, $m_{cat.}$ (Y_2O_3/Cu) = 2.9 mg

Table S5. Raw data of activation energy results for various catalysts.

Catalysts	Temperature (°C)	1000/(t+273)	CO_2 conv. (%)	Flow (mL/min)	Rate (mol/s/gcat)	Ln(Rate)
Cu/Y_2O_3	480	1.33	13.41	36.0	2.51E-05	-10.59
	500	1.29	11.55	60.0	3.66E-05	-10.22
	520	1.26	14.72	60.0	4.90E-05	-9.92
	540	1.23	14.63	80.0	8.26E-05	-9.40
Y_2O_3/Cu	460	1.36	10.61	43.9	1.56E-04	-8.76
	480	1.33	10.34	59.5	2.06E-04	-8.49
	500	1.29	11.16	74.0	2.77E-04	-8.19
	520	1.26	10.09	97.2	3.29E-04	-8.02

Notes: $m_{cat.}$ (Cu/Y_2O_3) = 10.0 mg, $m_{cat.}$ (Y_2O_3/Cu) = 5.1 mg, CO select. = 100%, 23%CO_2/69%H_2/8%N_2

Reference

1 X. Zhang, X. Zhu, L. Lin, S. Yao, M. Zhang, X. Liu, X. Wang, Y. Li, C. Shi and D. Ma, *ACS Catal.*, 2017, ***7***, 912.
2 A. M. Bahmanpour, F. Héroguel, M. Kilic, C. J. Baranowski, L. Artiglia, U. Röthlisberger, J. S. Luterbacher and O. Kröcher, *ACS Catal.*, 2019, ***9***, 6243.
3 X. Chen, X. Su, H. Duan, B. Liang, Y. Huang and T. Zhang, *Catal. Today*, 2017, ***281***, 312.
4 G. Kim, S. H. Ryu, H. Jeong, Y. Choi, S. Lee, J. H. Choi and H. Lee, *Angew. Chem. Int. Edit.*, 2023, e202306017.
5 Y. Yu, R. Jin, J. Easa, W. Lu, M. Yang, X. Liu, Y. Xing and Z. Shi, *Chem. Commun.*, 2019, ***55***, 4178.
6 Y. Shen, Z. Xiao, J. Liu and Z. Wang, *Chemcatchem*, 2019, ***11***, 5439.
7 A. Jia, S. Jiang, J. Lu and M. Luo, *J. Phys. Chem. C*, 2010, ***114***, 21605.
8 H. Yan, C. Yang, W. Shao, L. Cai, W. Wang, Z. Jin and C. Jia, *Nat. Commun.*, 2019, ***10***, 3470.
9 K. Xu, C. Ma, H. Yan, H. Gu, W. Wang, S. Li, Q. Meng, W. Shao, G. Ding, F. R. Wang and C. Jia, *Nat. Commun.*, 2022, ***13***, 2443.